# Bending Induced Temperature Increases in Double-Clad Fibers for High-Power Fiber Lasers

## Yoshito Shuto

Ofra Project, Iruma City, Japan

**Email address:**

ofra@tuba.ocn.ne.jp

**Abstract:** Rare-earth-doped optical fibers are one of the most promising solid-state lasers. In these fiber lasers, a cladding-pumping scheme using large-mode-area double-clad fibers (DCFs) is utilized to increase the overall conversion efficiency of pumping light and to overcome the restriction owing to the onset of stimulated Raman scattering. On the other hand, it is extremely challenging to increase the fiber core size while retaining the excellent beam quality because fibers with large core size allow propagation of several higher-order modes (HOMs), except for the fundamental mode (FM). In order to suppress HOMs, DCFs are bent with a relatively small bend radius. Failures at bends in an optical fiber are caused by light leaking from the core when the fiber is accidentally bent tightly with a high power input. For the DCFs with core radii of 10 and 20 µm, the relationship between the bending induced temperature increases and the bend losses in the bent DCFs was investigated theoretically by the explicit finite-difference method using the thermochemical $SiO_x$ production model. The temperature at the boundary between the inner and outer cladding layers increased with increasing optical power $P$ at 1.080 µm and was a large value higher than the softening temperature $T_s$ of the silica glass when $P$ = 5 kW was entered to the bent DCF with a bend radius $R$ of 150 mm and a core radius of 10 µm. On the other hand, the temperature at the boundary was a small value lower than the $T_s$ when $P$ = 10 kW was entered to the bent DCF with a large $R$ of 245-275 mm. Furthermore, it was found that the initiation of the fiber fuse was fairly easy under a certain conditions where the temperature at the boundary was higher than the $T_s$.

**Keywords:** Fiber Laser, Bending Loss, Fiber Fuse Phenomenon, Double-Clad Fiber, Finite-Difference Technique

## 1. Introduction

Rare-earth-doped optical fibers are one of the most promising solid-state lasers for efficient diode-pumped high power continuous-wave (CW) and fiber chirped-pulse amplification (CPA) laser systems. The output power from the ytterbium (Yb)-doped fiber lasers has abruptly increased over the past decade [1-6]. The overall conversion efficiencies are limited by the launch efficiency of the pump beam into the single-mode fiber core. High conversion efficiencies from pump light are obtained in Yb-doped silica fibers by using a cladding-pumping scheme [7] to ensure that virtually all of the incident pump power is absorbed in the doped fiber core. The cladding-pumping scheme can be realized using double-clad fibers (DCFs). In a double-clad configuration, light focused into the inner cladding is absorbed by the Yb-doped fiber core as the pump light proceeds down the fiber. This allows the use of multimode pump sources and relatively simple focusing systems for efficient coupling.

To overcome the restriction owing to the onset of stimulated Raman scattering (SRS), large-mode-area (LMA) fibers [8, 9] are utilized as DCFs. Typical LMA fibers used in the CW laser operation have core diameters of 20-40 µm and a numerical aperture (NA) of < 0.09 [10-14]. High output power of > 200 W in the CW laser operation has been reported using cladding-pumped Yb-doped and/or Nd-and Yb-codoped LMA fibers [10-27].

On the other hand, it is extremely challenging to increase the fiber core size while retaining the excellent beam quality because fibers with large core size allow propagation of several transversal modes, except for the fundamental mode (FM). As a result, the beam quality of these fibers is influenced by the existence of a higher-order mode (HOM). It is well known as transverse mode instability (TMI) [28] that the output beam profile in a Yb-doped optical fiber fluctuates in a seemingly chaotic way between the FM and

one (or more) HOM above threshold power. In order to suppress HOMs, Jeong *et al.* controlled a bend radius of the DCF and found that the bend loss of $LP_{11}$ mode reached ~1 dB/m for a bend radius of 12 cm, whereas that of $LP_{01}$ mode was less than ~0.04 dB/m [14].

It is well known that failures at bends in an optical fiber are caused by light leaking from the core when the fiber is accidentally bent tightly with a high power input [29-37]. Two kinds of failure regimes have been classified by Sikora *et al.*, which they named regime 1 (R1) and regime 2 (R2) failures [31]. Among them, R1 failure will lead to the catastrophic failure of the fiber and burning of the coating [32, 37]. As the transmittance of the coating material is not 100%, the leaked light is somewhat absorbed and heat occurs in the coating. Heat generated in the coating material by absorbing an optical power will be transferred to the neighboring cladding (silica glass) layer. When the temperature of the silica glass reaches higher than 1,100°C (= 1,373 K), the glass will soften and viscously deforming of the glass will occur [31, 32]. The fiber at the heating part will begin to kink sharply after the viscous deformation of the glass and the catastrophic failure of the fiber will occur. In the coating, the coating material is pyrolyzed at lower temperature than 1,100°C and charred after burning at high temperatures [32]. Furthermore, Kurokawa observed the generation of a fiber fuse when the bend diameter was 13 mm in a conventional single-mode optical fiber when the input power was 9 W at a wavelength of 1.48 μm [37].
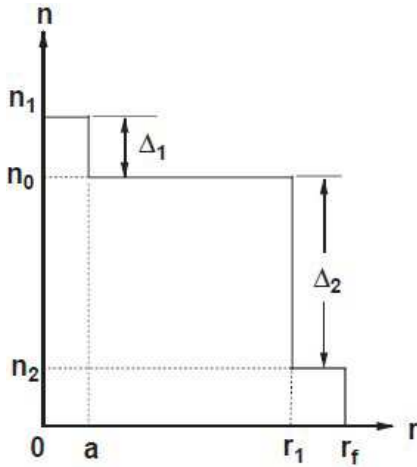
**Figure 1.** *Refractive-index profile of the DCF.*

An allowable curvature radius of the bent DCFs is not clear to prevent the R1 failure and/or the generation of fiber fuse phenomenon at the moment.

In this article, the relationship between the bending induced temperature increases and the bend losses in the bent DCFs was investigated in order to improve the reliability of DCFs for high-power fiber lasers.

## 2. Characteristics of DCFs

The refractive-index profile of the DCFs used in the calculation is shown in Figure 1. In this figure, $n_0$, $n_1$, and $n_2$ are the refractive indices in the core, inner cladding, and outer cladding, respectively.

The relative refractive-index differences $\Delta_1$ and $\Delta_2$ are defined as

$$\Delta_1 = \frac{(n_1^2 - n_0^2)}{2n_1^2} \sim \frac{(n_1 - n_0)}{n_1} \tag{1}$$

$$\Delta_2 = \frac{(n_0^2 - n_2^2)}{2n_0^2} \sim \frac{(n_0 - n_2)}{n_0} \tag{2}$$

The DCFs have a 20- and 40-μm-diameter Yb-doped silica glass core, a 400-μm-diameter inner cladding, and a 500-μm-diameter outer cladding consisting of a low-refractive-index polymer [10, 13, 14, 38].

**Table 1.** *Parameters of the DCFs.*

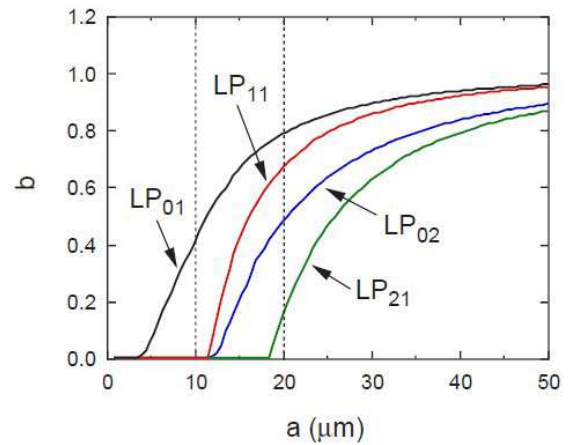| Parameters | Unit | DCF10 | DCF20 |
|---|---|---|---|
| $\Delta_1$ | % | 0.030 | 0.030 |
| $\Delta_2$ | % | 5.50 | 5.50 |
| $a$ | μm | 10 | 20 |
| $r_1$ | μm | 200 | 200 |
| $r_f$ | μm | 250 | 250 |
| $A_{eff}$ | μm² | 477 | 893 |

**Figure 2.** *Normalized propagation constants of FM and HOMs of Yb-doped DCF as a function of core radius with $\Delta_1 = 0.030\%$ and $\lambda_0 = 1.08$ μm.*

The parameters of the DCFs used in the calculation are shown in Table 1. In the following, the DCFs with $a = 10$ and 20 μm are referred to as DCF10 and DCF20, respectively.

Figure 2 shows the relationship between the core radius $a$ and the normalized propagation constant $b$ of FM ($LP_{01}$ mode) and/or HOMs ($LP_{11}$, $LP_{02}$ and $LP_{21}$ modes) of a Yb-doped DCF at $\lambda_0 = 1.08$ μm.

The normalized propagation constant $b$ is defined as

$$b = \frac{(n_e^2 - n_0^2)}{(n_1^2 - n_0^2)} \tag{3}$$

where $n_e$ is the effective index of propagation constant in the core. In Figure 2, the $\Delta_1$ of the Yb-doped core and the diameter of inner cladding were assumed to 0.030% and 400 μm, respectively. As shown in Figure 2, only the FM ($LP_{01}$ mode) exists in the core when $a = 10$ μm and the FM and two HOMs ($LP_{11}$ and $LP_{02}$ modes) exist mainly in the core when $a = 20$ μm at $\lambda_0 = 1.08$ μm.

## 3. Bending Loss in DCFs

The bending loss problem in the slab waveguides and optical fibers has been investigated by several research institutes [39-47]. When a step-index profile DCF is homogeneously curved with a bending raius $R$, as shown in Figure 3, the bending loss occurs in the core and the optical power losed in the core is emitted from the outer interface (or boundary) between the inner cladding (silica glass) and outer cladding (low-index polymer) layers.
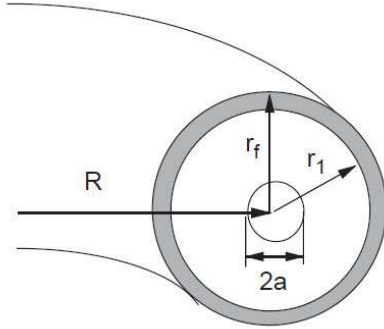


*Figure 3. Schematic view of a curved DCF.*

The bending loss $\alpha_B$ formula for $LP_{\mu v}$ modes in a step-index profile optical fibers is given by [47, 48]

$$\alpha_B = \frac{\sqrt{\pi}\, u^2}{s_\mu v^2 w^{\frac{3}{2}} K_{\mu+1}(w) K_{\mu-1}(w) \sqrt{Ra}} exp\left[-\frac{4w^3 R\Delta_1}{3v^2 a}\right] \quad (4)$$

where $s_\mu = 2$ for $\mu = 0$ and $s_\mu = 1$ for $\mu \neq 0$. $K_\mu$ is a modified Bessel function of order $\mu$, $R$ is the radius of curvature, and $a$ is the core radius. Parameters of $v$, $w$, and $u$ are given by

$$v = a\, k_0\, \sqrt{n_1^2 - n_0^2} \quad (5)$$

$$w = a\, k_0\, \sqrt{n_e^2 - n_0^2} \quad (6)$$

$$u = a\, k_0\, \sqrt{n_1^2 - n_e^2} \quad (7)$$

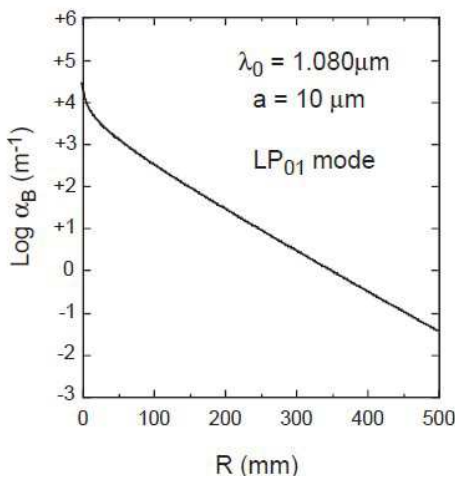where $k_0\ (= 2\pi / \lambda_0)$ is the wavenumber of light at the wavelength $\lambda_0$.



*Figure 4. Bending loss of $LP_{01}$ mode of DCF10 as a function of curvature radius with $\lambda_0 = 1.08\ \mu m$.*

The relationship between $R$ and $\alpha_B$ of the DCF10 and DCF20 was investigated using Eq. (3). The calculated results are shown in Figures 4 and 5. As shown in Figure 4, $\alpha_B$ decreases with increasing $R$. $\alpha_B$ reaches about 100 m$^{-1}$ at $R$ ~150 mm, and it attains about 10 m$^{-1}$ at $R$ ~245 mm.

Figure 5 shows the relationship between $R$ and $\alpha_B$ of the DCF20 at $\lambda_0 = 1.08\ \mu m$. In the DCF20, the FM ($LP_{01}$ mode) and two HOMs ($LP_{11}$ and $LP_{02}$ modes) exist mainly in the core (see Figure 2). As shown in Figure 5, the $\alpha_B$ values of all modes decrease with increasing $R$.
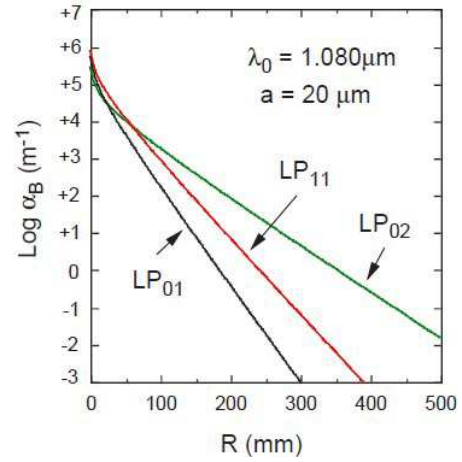


*Figure 5. Bending loss of $LP_{01}$, $LP_{11}$, and $LP_{02}$ modes of DCF20 as a function of curvature radius with $\lambda_0 = 1.08\ \mu m$.*

Table 2 shows the estimated $R$ values of all modes of DCF20 at $\alpha_B = 100$ m$^{-1}$ and 10 m$^{-1}$.

*Table 2. R values of the DCF20.*

| Modes | R (mm) at 100 m$^{-1}$ | R (mm) at 10 m$^{-1}$ |
|-------|------------------------|------------------------|
| $LP_{01}$ | ~110 | ~145 |
| $LP_{11}$ | ~145 | ~195 |
| $LP_{02}$ | ~195 | ~275 |

As shown in Table 2, $\alpha_B$ reaches about 100 m$^{-1}$ at $R$ = 110-195 mm, and it attains about 10 m$^{-1}$ at $R$ = 145-275 mm. The $R$ values of the HOMs ($LP_{11}$ and $LP_{02}$ modes) are larger than that of the FM ($LP_{01}$ mode) in the DCF20.

In the following section, the unsteady-state thermal conduction process in the DCFs is described theoretically by the explicit finite-difference method on the basis of the thermochemical $SiO_x$ production model [49].

## 4. Heat Conduction Calculation in DCFs

When a step-index profile DCF is homogeneously curved with a bending radius $R$, light leaking from the core transmits through the outer cladding (low-index polymer) layer. As the transmittance of low-index polymer at $\lambda_0 = 1.08\ \mu m$ is 94-96% [50], the leaked light is somewhat absorbed in the low-index polymer, and heat occurs in the polymer. Heat generated in the outer cladding (low-index polymer) layer by absorbing an optical power will be transferred to the neighboring inner cladding (silica glass) layer, as shown in Figure 6.
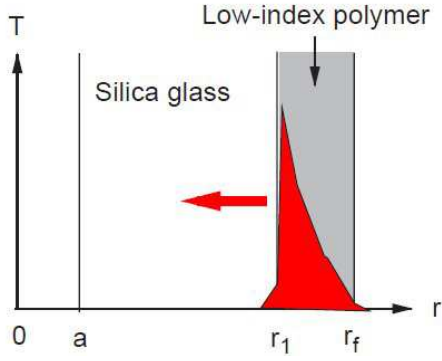
**Figure 6.** *Schematic view of heat conduction in a curved DCF.*

The one-dimensional unsteady heat conduction equation when a heat source is applied to the outer cladding (low-index polymer) layer in the curved DCF is given by

$$\frac{\partial T}{\partial t} = \frac{k}{\rho C_p}\frac{\partial^2 T}{\partial r^2} + \frac{\dot{Q}}{\rho C_p} \tag{8}$$

where $\kappa$, $\rho$, and $C_p$ are the thermal conductivity, density, and specific heat, respectively.

The heat source $\dot{Q}$ in Eq. (8) is the heat generation due to light absorption and is given by

$$\dot{Q} = \alpha_B\left(1 - t_p\right)I \tag{9}$$

where $\alpha_B$ is the bending loss and $t_p$ (= 96%) is the transmittance of low-index polymer at $\lambda_0 = 1.08$ μm. $I$ is the optical power density of the core and can be calculated by dividing the incident light power $P$ by the effective cross-sectional area $A_{eff}$ of the DCF at $\lambda_0 = 1.08$ μm.

The temperature distribution of the core, inner cladding, and outer cladding layers in the curved DCFs was investigated with the explicit finite-difference method. It was assumed that the DCF was in an atmosphere of $T = 298$ K and $r_1$ of the DCF was 200 μm (see Table 1). The area in the numerical calculation had a length of 2 mm in the radial ($r$) direction. There was 4,000 division in the $r$ direction and the calculation time interval was set to 1 ns.

It is well known that UV-curable low-index polymer is pyrolyzed at about 500°C [50] and charred at high temperatures. Therefore, in the heat conduction calculation, the following values of $\kappa$ (W m$^{-1}$ K$^{-1}$), $\rho$ (kg m$^{-3}$), and $C_p$ (J kg$^{-1}$ K$^{-1}$) in each temperature range were used.

(1) Parameters of low-index polymer in the temperature range from room temperature (298 K) to 773 K [51]:

$$C_p = 2,170$$

$$\kappa = 0.36$$

$$\rho = 1,700.$$

(2) Parameters of coal for $T > 773$ K [51]:
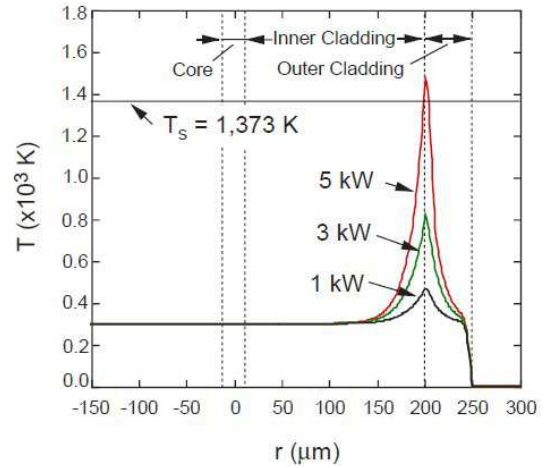
$$C_p = 1,260$$

$$\kappa = 0.28$$

$$\rho = 1,350.$$



**Figure 7.** *Temperature field in the curved DCF10 after 100 μs when P = 1-5 kW, $\alpha_B = 100$ m$^{-1}$, and $\lambda_0 = 1.08$ μm.*

The temperature field of the core, inner cladding, and outer cladding layers in the curved DCF10 along the $r$ direction was calculated at a time of 100 μs after the incidence of the 1-5 kW laser light when $\alpha_B = 100$ m$^{-1}$. The calculated result is shown in Figure 7.

As shown in Figure 7, the heat generated in the outer cladding layer is transferred to the neighboring cladding (silica glass) layer when laser power $P = 1-5$ kW is entered into the core of curved DCF10. The temperature at the boundary between the inner and outer cladding layers increases with increasing $P$ and reaches 1,470 K when $P = 5$ kW is entered to the curved DCF10. This temperature (1,470 K) is higher than the softening temperature $T_s$ (= 1,373 K [31, 32]) of the silica glass. When the temperature of the silica glass reaches higher than $T_s$, the fiber at the heating part will begin to kink sharply owing to the viscous deformation of the glass, and the catastrophic failure of the fiber will occur. Therefore, the curved DCFs with $\alpha_B = 100$ m$^{-1}$ cannot be utilized for high-power laser systems with output powers of > 5 kW.

Next, the temperature field of the core, inner cladding, and outer cladding layers in the curved DCF10 along the $r$ direction was calculated at a time of 100 μs after the incidence of the 1-10 kW laser light when $\alpha_B = 10$ m$^{-1}$. The calculated result is shown in Figure 8.
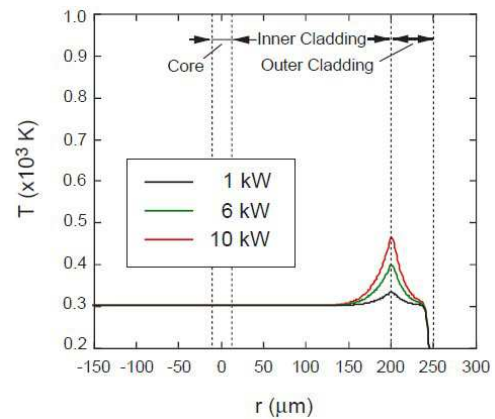


**Figure 8.** *Temperature field in the curved DCF10 after 100 μs when P = 1-10 kW, $\alpha_B = 10$ m$^{-1}$, and $\lambda_0 = 1.08$ μm.*

As shown in Figure 8, the heat generated in the outer cladding layer is slightly transferred to the inner cladding layer when laser power $P = 1$-10 kW is entered into the core of curved DCF10. The temperature at the boundary between the inner and outer cladding layers increases with increasing $P$ and reaches 460 K when $P = 10$ kW is entered to the curved DCF10. This temperature (460 K) is lower than the softening temperature $T_s$ (= 1,373 K) of the silica glass. Therefore, the curved DCFs with $\alpha_B = 10$ m$^{-1}$ can be utilized for high-power laser systems with output powers of 10 kW and below.

When step-index profile DCFs are homogeneously curved with a bending radius $R$, $\alpha_B$ reaches about 10 m$^{-1}$ at $R$ ~245 mm (DCF10) or $R = 145$-275 mm (DCF20). From the result described above, it is recommended that the operator must pay much attention to keep a large $R$ of > 245 mm (DCF10) or 275 mm (DCF20) when the DCFs are curved to be stored in the apparatus for high-power laser systems.

# 5. Fiber Fuse Generation in DCFs

When the temperature of the silica glass in a curved DCF reaches higher than $T_s$, the fiber at the heating part will begin to kink sharply owing to the viscous deformation of the glass, as shown in Figure 9.

As the curvature radius $R_k$ at a kink is smaller than the original bending radius $R$, the bending loss $\alpha_B$ at the kink is larger than that of the DCF curved with $R$. Heat generated at the boundary between the inner and outer cladding layers by absorbing the leaked light is directly proportional to $\alpha_B$, as shown in Eq. (9). Therefore, a lot of heat will be generated at the kinks and will be accumulated in the inner cladding and core layers. If heat accumulated in the core layer is sufficient for the generation and propagation of a fiber fuse, the fiber fuse phenomenon will be observed in the curved DCF.

As shown in Figure 7, the temperature at the boundary between the inner and outer cladding layers reaches 1,470 K when $P = 5$ kW is entered to the DCF10 curved with $R$ ~150 mm. As this temperature (1,470 K) is higher than the softening temperature $T_s$ (= 1,373 K) of the silica glass, the fiber at the heating part begins to kink sharply owing to the viscous deformation of the glass.
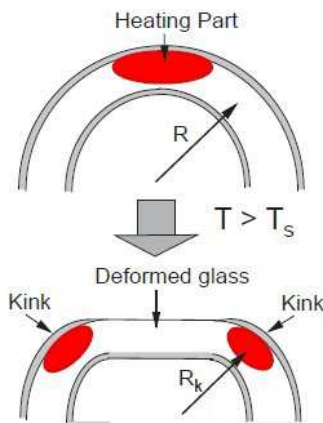


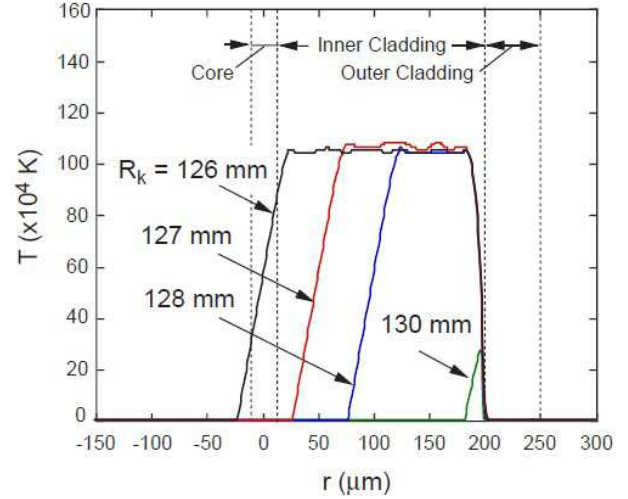**Figure 9.** *Schematic view of deformation of glass in the curved DCF.*



**Figure 10.** *Temperature field in the curved DCF10 after 100 μs when $R_k$ = 126-130 mm, $P = 5$ kW, and $\lambda_0 = 1.08$ μm.*

The temperature field of the core, inner cladding, and outer cladding layers in the curved DCF10 along the $r$ direction was investigated when the curvature radius $R_k$ at the kink was changed from 130 mm to 126 mm. The calculated result is shown in Figure 10.

As shown in Figure 10, the heat generated in the outer cladding layer is transferred to the neighboring cladding layer when laser power $P = 5$ kW is entered into the core of curved DCF10. The temperature near the boundary between the inner and outer cladding layers reaches $2.7 \times 10^5$ K when $R_k = 130$ mm. This temperature increases rapidly with decreasing $R_k$ and reaches about $1 \times 10^6$ K when $R_k = 126$-128 mm. A high-temperature region is spread over the whole inner cladding layer when $R_k = 126$ mm.

The temperature $T_c$ of core center reaches $5.4 \times 10^5$ K when $R_k = 126$ mm. This temperature is higher than the thermal decomposition temperature (~3,000 K) of the silica glass. In order to initiate a fiber fuse, a high temperature of 2,900 K and above is needed [49]. Therefore, the fiber fuse phenomenon will occur in the curved DCF10 with $R_k = 126$ mm when $P = 5$ kW and $\lambda_0 = 1.08$ μm.

As this $R_k$ (126 mm) at the kink is 0.84 times the original $R$ (= 150 mm), the initiation of the fiber fuse will be fairly easy under a certain conditions where the temperature at the boundary between the inner and outer cladding layers is higher than the softening temperature $T_s$ of the silica glass.

# 6. Conclusion

For the large-mode-area double-clad fibers (DCFs) with core radii of 10 and 20 μm, the relationship between the bending induced temperature increases and the bend losses in the bent DCFs was investigated theoretically by the explicit finite-difference method using the thermochemical SiO$_x$ production model. The temperature at the boundary between the inner and outer cladding layers increased with increasing optical power $P$ at 1.080 μm and was a large value higher than the softening temperature $T_s$ of the silica glass when $P = 5$ kW was entered to the bent DCF with a bend radius $R$ of 150 mm

and a core radius of 10 μm. On the other hand, the temperature at the boundary was a small value lower than the $T_s$ when $P =$ 10 kW was entered to the bent DCF with a large $R$ of 245-275 mm. Furthermore, it was found that the initiation of the fiber fuse was fairly easy under a certain conditions where the temperature at the boundary was higher than the $T_s$.

# References

[1] Richardson D. J., Nilsson J., and Clarkson W. A. (2010). High power fiber lasers: current status and future perspectives. J. Opt. Soc. Am. B, 27 (11), B63-B92.

[2] Tünnermann A., Schreiber T., and Limpert J. (2010). Fibre lasers and amplifiers: an ultrafast performance evolution. Appl. Opt., 49 (25), F71-F78.

[3] Jauregui C., Limpert J., and Tünnermann A. (2013). High-power fibre lasers. Nat. Photonics, 7, 861-867.

[4] Fermann M. E. and Hartl I. (2013). Ultrafast fibre lasers. Nat. Photonics, 7, 868-874.

[5] Zervas M. N. and Codemand C. A. (2014). High power fiber lasers: a review. IEEE J. Selected Topics Quantum Electron., 20 (5), 0904123.

[6] Shi W., Fang Q., Zhu X., Norwood R. A., and Peyghambarian N. (2014). Fiber lasers and their applications. Appl. Opt., 53 (28), 6554-6568.

[7] Snitzer E., Po H., Hakimi F., Tumminelli R., and McCollum B. C. (1988). Double clad, offset core Nd fiber laser. Conf. on Optical Fiber Sensors, PD5-1.

[8] Broderick N. G. R., Offerhaus H. L., Richardson D. J., Sammut R. A., Caplen J., and Dong L. (1999). Large mode area fibers for high power applications. Opt. Fiber Technol., 5, 185-196.

[9] Alvarez-Chavez J. A., Offerhaus H. L., Nilsson J., Turner P. W., Clarkson W. A., and Richardson D. J. (2000). High-energy, high-power ytterbium-doped Q-switched fiber laser. Opt. Lett., 25 (1), 37-39.

[10] Jeong Y., Sahu J. K., Williams R. B., Richardson D. J., Furusawa K., and Nilsson J. (2003). Ytterbium-doped large-core fibre laser with 272 W output power. Electron. Lett., 39 (13), 977-978.

[11] Limpert J., Liem A., Zellmer H., and Tünnerman A. (2003). 500 W continuous-wave fibre laser with excellent beam quality. Electron. Lett., 39 (8), 645-647.

[12] Liu C.-H., Ehlers B., Doerfel F., Heinemann S., Carter A., Tankala K., Farroni J., and Galvanauskas A. (2004). 810 W continuous-wave and single-transverse-mode fibre laser using 20 μm core Yb-doped double-clad fibre. Electron. Lett., 40 (23), 1471-1472.

[13] Jeong Y., Sahu J. K., Payne D. N., and Nilsson J. (2004). Ytterbium-doped large-core fibre laser with 1 kW of continuous-wave output power. Electron. Lett., 40 (8), 470-471.

[14] Jeong Y., Sahu J. K., Payne D. N., and Nilsson J. (2004). Ytterbium-doped large-core fiber laser with 1.36 kW continuous-wave output power. Opt. Express, 12 (25), 6088-6092.

[15] He B., Zhou J., Lou Q., Xue Y., Li Z., Wang W., Dong J., Wei Y., and Chen W. (2010). 1.75-kilowatt continuous-wave output fiber laser using homemade ytterbium-doped large-core fiber. Microwave Opt. Technol. Lett., 52 (7), 1668-1671.

[16] Jeong Y., Boyland A. J., Sahu J. K., Chung S., Nilsson J., and Payne D. N. (2009). Multi-kilowatt single-mode ytterbium-doped large-core fiber laser. J. Opt. Soc. Korea, 13 (4), 416-422.

[17] Huang L., Wang W., Leng J., Guo S., Xu X., and Cheng X. (2014). Experimental investigation on evolution of the beam quality in a 2-kW high power fiber amplifier. IEEE Photon. Technol. Lett., 26 (1), 33-36.

[18] Khitrov V., Minelly J. D., Tumminelli R., Petit V., and Pooler E. S. (2014). 3 kW single-mode direct diode-pumped fiber laser. Proc. Soc. Photo-Opt. Instrum. Eng., 8961, 89610V-1-89610V-6.

[19] Yu H., Zhang H., Lv H., Wang X., Leng J., Xiao H., Guo S., Zhou P., Xu X., and Chen J. (2015). 3.15 kW direct diode-pumped near diffraction-limited all-fiber-integrated fiber laser. Appl. Opt., 54 (14), 4556-4560.

[20] Beier F., Hupel C., Nold J., Kuhn S., Hein S., Ihring J., Sattler B., Haarlammert N., Schreiber T., Eberhardt R., and Tünnermann A. (2016). Narrow linewidth, single mode 3 kW average power from a directly diode pumped ytterbium-doped low NA fiber amplifier. Opt. Express, 24 (6), 6011-6020.

[21] Beier F., Hupel C., Kuhn S., Hein S., Nold J., Proske F., Sattler B., Liem A., Jauregui C., Limpert J., Haarlammert N., Schreiber T., Eberhardt R., and Tünnermann A. (2017). Single mode 4.3 kW output power from a diode-pumped Yb-doped fiber amplifier. Opt. Express, 25 (13), 14892-14899.

[22] Su R., Tao R., Wang X., Zhang H., Ma P., Zhao P., and Xu X. (2017). 3.7 kW monolithic narrow linewidth single mode fiber laser through simultaneously suppressing nonlinear effects and mode instability. Laser Phys. Lett., 14, 085102.

[23] Wang Y., Gao C., Tang X., Zhan H., Peng K., Ni L., Liu S., Li Y., Guo C., Wang X., Zhang L., Yu J., Jiang L., Lin H., Wang J., Jing F., and Lin A. (2018). 30/900 Yb-doped aluminophosphosilicate fiber presenting 6.85-kW laser output pumped with commercial 976-nm laser diodes. IEEE J. Lightwave Technol., 36 (16), 3396-3402.

[24] Xiao Q., Li D., Huang Y., Wang X., Wang Z., Tian J., Yan P., and Gong M. (2018). Directly diode and bi-directional pumping 6 kW continuous-wave all-fibre laser. Laser Phys., 28, 125107.

[25] Shima K., Ikoma S., Uchiyama K., Takubo Y., Kashiwagi M., and Tanaka D. (2018). 5-kW single stage all-fiber Yb-doped single-mode fiber laser for material processing. Proc. Soc. Photo-Opt. Instrum. Eng., 10512, 105120C-1-105120C-6.

[26] Lin H., Xu L., Li C., Shu Q., Chu Q., Xie L., Guo C., Zhao P., Li Z., Wang J., Jing F., and Tang X. (2019). 10.6 kW high-brightness cascade-end-pumped monolithic fiber lasers directly pumped by laser diodes in step-index large mode area double cladding fiber. Results in Phys., 14, 102479.

[27] Ye Y., Yang B., Wang P., Zeng L., Xi X., Shi C., Zhang H., Wang X., Zhou P., and Xu X. (2021). Industrial 6 kW high-stability single-stage all-fiber laser oscillator based on conventional large mode area ytterbium-doped fiber. Laser Phys., 31, 035104.

[28] Jauregui C., Stihler C., and Limpert J. (2020). Transverse mode stability. Ad. Opt. Photon., 12 (2), 420-484.

[29] Percival R. M., Sikora E. S. R., and Wyatt R. (2000). Catastrophic damage and accelerated aging in bent fibres caused by high optical powers. Electron. Lett., 36 (5), 414-415.

[30] Logunov S. L. and DeRosa M. E. (2003). Effect of coating heating by high power in optical fibres at small bend diameters. Electron. Lett., 39 (12), 897-898.

[31] Sikora E. S. R., McCartney D. J., Farrow K., and Davey R. (2003). Reduction in fibre reliability due to high optical power. Electron. Lett., 39 (14), 1043-1044.

[32] Glaesemann G. S., Chien C., Clark D. A., Coon J., DeMartino S. E. and Logunov S. L. (2004). Analysis of optical fiber failures under bending and high power. Proc. Soc. Photo-Opt. Instrum. Eng., 5465, 1-10.

[33] Davis I. M., Glaesemann G. S., Ten S., and Winningham M. J. (2005). Optical fibres resilient to failure in bending under high power. Proc. European Conf. Opt. Commun. (ECOC 2005), We. 3.4.5, 471-472.

[34] Bigot-Astruc M., Sillard P., Gauchard S., Le Roux P., and Brandon E. (2006). Analysis of coating temperature increase in fibers under high power and tight bending. Proc. Opt. Fiber Commun. Conf. (OFC 2006), OFK4.

[35] Sikora E. S. R., McCartney D. J., and Wright J. V. (2007). Impact of coating ageing on susceptibility to high-power damage at fibre bends. Electron. Lett., 43 (4), 208-210.

[36] Logunov S. L., Chien C.-K., and Clark D. A. (2009). High power laser damage of standard and bent resistant fibres. Electron. Lett., 45 (20), 1019-1020.

[37] Kurokawa K. (2012). Optical fiber for high-power optical communication. Crystals, 2, 1382-1392.

[38] Kim J. W., Shen D. Y., Sahu J. K.., and Clarkson W. A. (2009). Fiber-laser-pumped Er: YAG lasers. IEEE J. Selected Topics Quantum Electron., 15 (2), 361-371.

[39] Marcatili E. A. J. (1969). Bends in optical dielectric guides. Bell Syst. Tech. J., 48, 2103-2132.

[40] Marcatili E. A. J. and Miller S. E. (1969). Improved relations describing directional control in electromagnetic wave guidance. Bell Syst. Tech. J., 48, 2161-2188.

[41] Marcuse D. (1971). Bending losses of the asymmetric slab waveguide. Bell Syst. Tech. J., 50, 2551-2563.

[42] Gloge D. (1972). Bending loss in multimode fibers with graded and ungraded core index. Appl. Opt., 11 (11), 2506-2513.

[43] Lewin L. (1974). Radiation from curved dielectric slabs and fibers. IEEE Trans. Microwave Theory and Techniques, MTT-22 (7), 718-727.

[44] Kuester E. and Chang D. C. (1975). Surface-wave radiation loss from curved dielectric slabs and fibers. IEEE J. Quantum Electron., QE-11 (11), 903-907.

[45] Marcuse D. (1976). Curvature loss formula for optical fibers. J. Opt. Soc. Am., 66 (3), 216-220.

[46] Marcuse D. (1976). Field deformation and loss caused by curvature of optical fibers. J. Opt. Soc. Am., 66 (4), 311-320.

[47] Sakai J. and Kimura T. (1978). Bending loss of propagation modes in arbitrary-index profile optical fibers. Appl. Opt., 17 (10), 1499-1506.

[48] Sakai J. (2004). Waveguide Optics, Chap. 12, Kyoritsu Shuppan Co.. Ltd., Tokyo.

[49] Shuto Y. (2014). Heat conduction modeling of fiber fuse in single-mode optical fibers. J. Photonics, 2014, 645207.

[50] Product information of UV-curable low-index resin, DIC Corporation.

[51] Shoji M. (1995). Heat Transfer Textbook, Appendix F, University of Tokyo Press, Tokyo.